

Fast Deep Hedging with Second-Order Optimization

Konrad Mueller

Imperial College London
J.P. Morgan
London, UK

Lukas Gonon*

Imperial College London
London, UK

Amira Akkari*

J.P. Morgan
London, UK

Ben Wood*

J.P. Morgan
London, UK

ABSTRACT

Hedging exotic options in presence of market frictions is an important risk management task. Deep hedging can solve such hedging problems by training neural network policies in realistic simulated markets. Training these neural networks may be delicate and suffer from slow convergence, particularly for options with long maturities and complex sensitivities to market parameters. To address this, we propose a second-order optimization scheme for deep hedging. We leverage pathwise differentiability to construct a curvature matrix, which we approximate as block-diagonal and Kronecker-factored to efficiently precondition gradients. We evaluate our method on a challenging and practically important problem: hedging a cliquet option on a stock with stochastic volatility by trading in the spot and vanilla options. We find that our second-order scheme can optimize the policy in 1/4 of the number of steps that standard adaptive moment-based optimization takes.

CCS CONCEPTS

• **Theory of computation** → **Stochastic control and optimization**; *Reinforcement learning*; *Nonconvex optimization*.

KEYWORDS

Deep Hedging, Cliquet, Second-Order Optimization, KFAC, Natural Gradient Descent

1 INTRODUCTION

Hedging financial derivatives is a fundamental risk management problem. Classical models provide solutions by relying on strong simplifying assumptions such as absence of market frictions. Deep hedging [6] approximates solutions to hedging problems by training a neural network to take optimal hedging decisions. Deep hedging has gained popularity in both academia and industry as it applies to hedging problems with an arbitrary contingent claim, market simulator, and hedging objective. For instance, deep hedging has been applied to lookback options [7] and extended to general initial portfolios [32], and non-Markovian [18] or uncertain [25] simulators. We refer to existing surveys [14, 34] for a comprehensive overview. In practice, learning to hedge exotic options is a challenging optimization on a high-dimensional action space that requires computing pathwise gradients at high backpropagation depth. Solving this optimization reliably and quickly is practically important,

especially when refitting models frequently to recalibrated simulators. Like most neural networks, deep hedging models are usually optimized with diagonally preconditioned gradient descent (e.g., Adam [21]). To improve optimization, we propose a *second-order* scheme that preconditions gradients with the inverse of a Kronecker-factored [28] curvature matrix.

The setting of our paper is a challenging and practically important hedging problem: hedging a *path-dependent* option by trading in the spot and vanilla options. While the focus of our paper lies on optimization, we start with a modification to the standard deep hedging framework to efficiently parameterize option hedging. We define a dynamically evolving action space such that puts and calls with the same moneyness and maturity are tradable on any path and at any time (floating grid). In this new formulation, representing the current hedging portfolio is challenging, but can be internalized into the neural network through recurrent connections.

We then focus on the deep hedging optimization. Fundamentally, the optimization is difficult because we can evaluate the model-free hedging error only when the contingent claim matures. This implies that (i) to compute loss and gradients we need to unroll the network over all time steps and (ii) credit assignment to individual hedging decision is difficult, especially since the environment is highly stochastic. To address these issues, we propose a second-order optimization scheme that builds on techniques from both reinforcement learning (RL) and the training of recurrent neural networks (RNNs). Many popular RL algorithms [20, 36, 40] are based on natural gradient descent [1] and precondition policy gradients with the inverse Fisher information matrix (FIM) of the action distribution. Preconditioning with the FIM can be made scalable with Kronecker-factored approximate curvature (KFAC) [28], which approximates the FIM as block-diagonal with Kronecker-factored blocks. In contrast to most RL problems, the deep hedging environment is differentiable, so we do not need to randomize actions and estimate gradients with the score function trick. Consequently, preconditioning with the FIM is not applicable.

Instead, we construct a preconditioner for the deep hedging problem that leverages the pathwise differentiable transition dynamics. Our preconditioner respects the curvature of the loss with respect to actions but linearizes the neural network. It is linked to the Hessian of the deep hedging problem, as it approximates a generalized Gauss Newton matrix [35]. We use the KFAC approximations [11, 27, 28] on our preconditioner to obtain a tractable algorithm. To stably invert the curvature matrix, we propose a new shrinkage-based damping scheme.

*Equal contribution

We compare the resulting second-order scheme with Adam on training a neural network to hedge a *cliquet* option in a stochastic volatility model. With Kronecker-factored preconditioning, the optimization progresses significantly faster per-iteration. This translates into a decrease in training time as additional computational costs can be amortized [3]. We analyze the learned strategy for hedging a cliquet and highlight the importance of using options as hedging instruments.

2 DEEP HEDGING

2.1 Hedging problem

We seek to approximately solve the problem of hedging an exotic equity derivative in finite, discrete time. We consider equidistant time steps $t \in \{0, 1, \dots, T\}$ up to a time horizon $T < \infty$, and random variables on a filtered probability space $(\Omega, \mathcal{F}, \mathbb{P})$. The filtration $\mathbb{F} = (\mathcal{F}_t)_{t \geq 0}$ is generated as $\mathcal{F}_t = \sigma(I_0, \dots, I_t)$, where I_t captures newly available market information at time t and takes values in \mathbb{R}^{d_t} . We denote \mathcal{F}_t -measurable random variables with subscript t .

Consider an underlying with $\mathbb{R}_{>0}$ -valued stock price process $(x_t)_{t \geq 0}$. At time $t = 0$ a bank sells a path-dependent derivative for a price $p_0 > 0$. The derivative has payoff $\psi(x)$ at time T for some $\psi : \mathbb{R}_{>0}^{T+1} \rightarrow \mathbb{R}$. At times $t \in \{0, \dots, T-1\}$, the bank chooses an \mathbb{R}^d -valued control (also ‘‘action’’) u_t , representing trades in d different hedging instruments. The first component $u_t^{(1)}$ is a trade in the underlying x ; other hedging instruments are European puts and calls on x . We therefore focus on hedging spot and volatility risk, and neglect other risk factors. In particular, we assume deterministic interest rates and treat prices and payments as discounted to $t = 0$. We highlight two different modeling choices for specifying which vanilla options are available for trade at any time t (let $i > 1$ below).

- (a) *Fixed grid:* $u_t^{(i)}$ is a trade in the same contract at each time t .
 - Example: If $u_t^{(i)}$ trades a call option with strike $K^i > 0$ and maturity τ_i , then $u_{t+1}^{(i)}$ trades the same call option with strike K^i and reduced time to maturity $\tau_i - 1$.
- (b) *Floating grid:* $u_t^{(i)}$ is a trade in an option with the same moneyness and time to maturity at each time t .
 - Example: For all t , $u_t^{(i)}$ is a trade in a call option with time to maturity $\tau_i > 0$ and strike $K_t^i = x_t \exp(k_i)$, with moneyness $k_i \in \mathbb{R}$.

Buehler et al. [6] use a fixed grid as they consider trading in the same d hedging instruments at all times. In this setting, we can unwind past trades and track the hedging portfolio

$$\partial_t = \sum_{s=0}^t u_s, \quad (1)$$

as the sum of past hedges. The fixed grid can accommodate all types of hedging instruments but assigns a new dimension to each tradable contract. To capture all relevant puts and calls on any path $(x_t)_{t \geq 0}$ and at any time t , we need to choose a large grid size d that depends increasingly on T .

The floating grid addresses this issue because at each time step we only need to represent the much smaller set of options that are relevant in the current state. This floating definition of the action space means that each option can only be traded once, implying

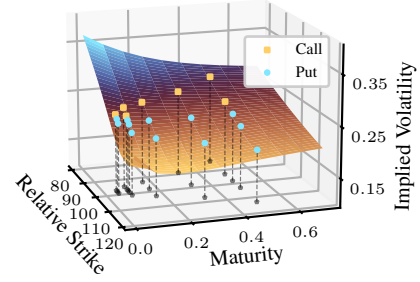


Figure 1: Floating grid. Implied volatility surface is stochastic; relative strike (in %) and maturity of tradable options are constant. Marked puts/calls are used in our experiments.

that all trades are held until maturity. However, a trader can approximately offset an option traded at time t in later trading, as long as the option remains within the relevant set.¹ The floating grid provides a reasonable representation of the typical range of available liquidity in practice. We do not focus on the details of translating a floating grid policy into real-world trades in this work.

We consider hedging on the floating grid with the convention that only out-of- or at-the-money options are available. If $k_i > 0$, the i th option is a call, and if $k_i \leq 0$, it is a put. We remove options that mature after T from the grid, i.e., set $u_t^{(i)} = 0$ when $\tau_i > T - t$.

Trades u_t increase or decrease the terminal PnL by $u_t^\top r_{t,T}$, where $r_{t,T}$ is the total return realized up to time T of the d instruments traded at time t . The total return of trading the underlying x , is given by $r_{t,T}^{(1)} = x_T - x_t$. For $i > 1$ and when the i th option is a call,

$$r_{t,T}^{(i)} = (x_{t+\tau_i} - K_t^i)^+ - C_t(\tau_i, k_i)$$

where $C_t(\tau_i, k_i)$ is the premium paid for the call at time t . Put option returns are defined analogously with payoff $(K_t^i - x_{t+\tau_i})^+$. All hedging leads to terminal gains (or losses) of

$$\Gamma_T(u) := \sum_{t=0}^{T-1} u_t^\top r_{t,T},$$

and incurs transaction costs. For simplicity, we consider proportional transaction costs that accumulate to

$$C_T(u) := \sum_{t=0}^{T-1} c^\top |u_t|,$$

where costs $c \in \mathbb{R}_{>0}^d$ are instrument-dependent, and $|\cdot|$ is applied elementwise. Hedges are determined by a *policy* π which is a collection of maps $(\pi_t)_{t < T}$ such that

$$u_t = \pi_t(I_0, \dots, I_t), \quad (2)$$

for all $t \in \{0, \dots, T-1\}$. We want to find a policy π that minimizes a given hedging objective, for which there are plenty of

¹For example consider buying a 40-day call at $t = 0$ with strike K_0^i . After 20 days we may offset the terminal payoff of this call option by selling a convex combination of two 20-day calls with $K_{20}^j \leq K_0^i \leq K_{20}^k$. This requires the availability of such calls.

well-motivated choices [5]. In this work, we focus on minimizing a weighted sum of PnL variance [37] and transaction costs

$$\gamma \mathbb{V}(\Gamma_T(u) - \psi(x)) + \mathbb{E}[C_T(u)], \quad (3)$$

where actions u are given via the policy π as in eq. (2). The risk aversion coefficient $\gamma > 0$ weighs the importance of low hedging error vs. low transaction cost.

Cliquet. Above, we described the problem of hedging a generic European payoff ψ . In our numerical experiments, we take ψ to be a *cliquet option*. Cliquets are traded in standard formats, and are simple to describe, but difficult to hedge because of their sensitivity to volatility dynamics. This makes them a good test case for deep hedging. We consider a standard form of the locally-capped, globally-floored cliquet option, which pays at maturity T

$$\psi(x) = \max \left[\sum_{\tau_i=\tau_1}^T \min \left(\frac{x_{\tau_i}}{x_{\tau_{i-1}}} - 1, \mu \right), 0 \right],$$

for reset dates $0 < \tau_1 < \dots < \tau_m = T$. In each of the m periods (typically of equal duration), we measure the return of the underlying asset, apply a cap at $\mu > 0$; we then sum these returns, and floor the result at zero. Intuitively, we can see that the contribution of the current period to the final payoff looks like a forward minus an option with moneyness (as of the period start) of $1 + \mu$. However, we do not know the moneyness of the equivalent option in the next period, or the effect of the global floor.

2.2 Parameterizing the hedging policy

Deep hedging [6] approaches the hedging problem by parameterizing the policy with a neural network and training it to minimize the hedging objective. Buehler et al. [6] use the fixed grid formulation, such that the path-dependence of optimal hedging decisions (eq. 2) reduces to a dependence on the portfolio ϑ_t when I is a Markov process. Then, they define the policy through the parameterization²

$$\vartheta_t = \pi_\theta(I_t, \vartheta_{t-1}), \quad (4)$$

where π_θ is a neural network with parameters $\theta \in \mathbb{R}^n$. We slightly abuse notation here and absorb time dependence into the information process (“ $I_t \leftarrow (I_t, t)$ ”). The network is recurrent in its output ϑ_t but does not have a conventional hidden state.

For hedging policies on the floating grid, this parameterization is not immediately applicable. There, trades u_t and u_s are in different contracts, so that the hedging portfolio cannot be computed as the sum of past hedges. The precise portfolio at time t can only be represented as a concatenation of past hedges $(u_s)_{s \leq t}$ and spot values $(x_s)_{s \leq t}$.³ Such a naive representation is high-dimensional (growing in T), sparse, and in our experience difficult to learn from. Instead of tracking the portfolio precisely, we represent it approximately as $h_t \in \mathbb{R}^k$ with $k \ll Td$. Reducing the dimension of the portfolio representation is less restrictive than reducing the dimension of the action space (e.g., using fixed grid with small d). On any given path most actions will be close to zero, such that the holdings’ effective dimension is low. This does not imply that these actions are useless; option hedging makes a significant contribution to the hedging performance (see section 4.2).

²On the fixed grid, having the network output u_t or ϑ_t is conceptually equivalent.

³The path of x is needed to track the strikes at which past options were traded.

Option portfolios are commonly represented via their Greeks [32], i.e., aggregated sensitivities of individual option prices with respect to market parameters. While low-dimensional, the Greeks representation is expensive to compute in black-box simulators and its compression may be limiting. Instead, we learn the representation through recurrent connections and consider parameterizations

$$(u_t, \{h_t^l\}_{l \leq L}) = \pi_\theta(I_t, u_{t-1}, \{h_{t-1}^l\}_{l \leq L}), \quad (5)$$

where h_t^l is the hidden state of one of L layers with a recurrent connection. Unlike standard recurrent architectures [10, 17], this parameterization is additionally recurrent in its outputs $(u_t)_{t < T}$. This recurrence helps the network memorize its output sequence: the network can write u_{t-1} to memory during the time t forward pass. All recurrent connections can also capture non-Markovianity in inputs $(I_t)_{t < T}$ [18]. Providing the last action as an input is commonly done when training LSTMs on RL problems.⁴ Removing the additional recurrence in u_t and treating deep hedging as a sequence modeling problem, is in our experience less efficient but could allow for parallelization with modern recurrent architectures [33].

2.3 Optimizing the hedging policy

With a given parameterization, the hedging problem reduces to a minimization problem on the parameter space \mathbb{R}^n , which can be solved with gradient-based optimization. The loss of eq. (3) is now a function $\mathcal{L}(\theta)$ of parameters, whose gradient can be estimated pathwise [31] as π_θ is differentiable in θ and the loss is pathwise differentiable in the network outputs $(u_t)_{t < T}$. Optimizing π_θ with stochastic gradient estimates and an optimizer such as Adam [21] works but can be challenging. A primary reason for this is that computing pathwise gradients requires backpropagating the error through time and unrolling π_θ for T times. Even for small neural networks, this is computationally expensive. The common mitigation strategy of truncating the backpropagation [19] is not applicable as the hedging loss is not *separable* over time: viewing the loss function (eq. 3) as a function of u , we can write the loss as

$$\sum_{t=0}^{T-1} \ell_t(u_t) + \ell_T \left(\sum_{t=0}^{T-1} u_t^\top r_{t,T} \right),$$

where the first term captures transaction costs. The second term captures the quadratic hedging error and is thereby non-linear in u and can only be computed at time T . This is in contrast to loss functions in supervised learning of type “ $\sum_t \ell(u_t, y_t)$ ”, where a component $\ell(u_t, y_t)$ can be evaluated immediately at time t . This difficulty is not specific to our loss function: evaluating any measure of hedging error at $t < T$ requires valuing the portfolio, which is model-dependent. The loss decomposition also points to an ill-conditioning issue: u_t impact the terminal loss component only through the weighted sum Γ_T , such that the *per-sample* hedging loss does not have a unique minimizer u . While common in RL, this is in contrast to supervised learning problems, where the “square can usually be found inside the sum”, i.e., $\ell(u_t, y_t) = (u_t - y_t)^2$.

Motivated by these observations, we propose a second-order optimization scheme for deep hedging. Our second-order method is

⁴When using pathwise gradients, gradients flow through the action recurrence. This is in contrast to training such networks with policy gradient methods.

more efficient on a per-step basis, addressing the large per-step cost due to the high backpropagation depth. We precondition gradient descent updates with a rich curvature matrix that addresses the quadratic loss component ℓ_T . We replace the implicit loss linearization of gradient descent with a second-order model that respects the curvature in ℓ_T and only linearizes the neural network π_θ .

3 SECOND-ORDER OPTIMIZATION FOR DEEP HEDGING

3.1 Second-order optimization of neural networks

Before discussing second-order optimization for deep hedging, we review the underlying concepts in a standard supervised learning setting [26, 30]. Given input x , a neural network f_θ outputs $z = f_\theta(x)$ to match a target y with loss $\mathcal{L}(\theta) = \mathbb{E}[\ell(f_\theta(x), y)]$. To minimize the loss, we model the loss landscape $\mathcal{L}(\theta + \delta)$ for steps $\delta \in \mathbb{R}^n$ around the current iterate θ as

$$M(\delta) = \mathcal{L}(\theta) + \nabla \mathcal{L}(\theta)^\top \delta + \frac{1}{2} \delta^\top B \delta,$$

for some symmetric matrix $B \in \mathbb{R}^{n \times n}$. If B is positive definite, M has a unique minimum at $\delta^* = -B^{-1} \nabla \mathcal{L}(\theta)$. This is proportional to the step chosen by gradient descent, Newton’s method, and natural gradient descent [1], when B is the identity, Hessian, or Fisher Information Matrix (FIM) respectively. In this work, we focus on the class of preconditioners \mathcal{B} introduced by Martens [26, sec. 12], where any $B \in \mathcal{B}$ is of the form

$$B = \mathbb{E}_{x,y} \left[J_{z,\theta}^\top(x) H(x, y, \theta) J_{z,\theta}(x) \right].$$

The distribution of x, y can be arbitrary. $J_{z,\theta}(x)$ is the Jacobian of the network output with respect to θ evaluated at $z = f_\theta(x)$. $H(x, y, \theta)$ takes values in $\mathbb{R}^{m \times m}$, is positive definite,⁵ and parameterization invariant [22, App. C]. Martens [26, sec. 12] showed that preconditioned gradient descent with any $B \in \mathcal{B}$ satisfies an approximate invariance property. The family \mathcal{B} generally does not contain the Hessian, but it includes the FIM, and the *extended* or *generalized Gauss-Newton* matrix (GGN) [35]. The GGN is a positive semi-definite (psd) approximation of the Hessian matrix and can be interpreted as the Hessian of $\mathcal{L}(\theta)$, when replacing the inner model function f_θ with a “linearization” [29]. Here, the GGN is the matrix

$$G = \mathbb{E}_{x,y} \left[J_{z,\theta}^\top(x) H_z(y) J_{z,\theta}(x) \right],$$

where $H_z(y)$ is the Hessian of $\ell(z, y)$ with respect to model outputs z . The GGN is psd as ℓ is assumed to be convex in z .

Practically, preconditioners \mathcal{B} are relevant because we can approximate them efficiently by imposing a Kronecker-product structure (see section 3.2). This Kronecker-factored approximation was first developed for the FIM [28] and exploits that the FIM is the uncentered covariance matrix of gradients. More generally, we can interpret any $B \in \mathcal{B}$ as a covariance matrix; not of the actual gradient, but of a random vector called the *pseudo-gradient* [12]. Specifically, since $H(x, y, \theta)$ is positive definite for any (x, y, θ) , it is the covariance matrix of the random vector LZ , where $LL^\top = H(x, y, \theta)$ and

Z has zero mean and identity covariance (e.g., standard Gaussian). Any $B \in \mathcal{B}$ can be written as the covariance matrix

$$B = \mathbb{E}_{x,y,Z} \left[\underbrace{J_{z,\theta}^\top(x) L(x, y, \theta)}_{\mathcal{D}\theta} Z \underbrace{\left(J_{z,\theta}^\top(x) L(x, y, \theta) Z \right)^\top}_{(\mathcal{D}\theta)^\top} \right],$$

of the random vector $\mathcal{D}\theta$. We can sample $\mathcal{D}\theta$ by sampling x, y, Z , computing $z = f_\theta(x)$, L , and *backpropagating* $\ell^{\text{pseudo}} = \langle z, LZ \rangle$. Consequently, we can define the pseudo-gradient $\mathcal{D}Y \in \mathbb{R}^{M \times N}$ for any matrix $Y \in \mathbb{R}^{M \times N}$ as $(\mathcal{D}Y)_{i,j} = \partial \ell^{\text{pseudo}} / \partial Y_{i,j}$.

3.2 Kronecker-factored approximations

Computing, storing, and inverting a dense preconditioner $B \in \mathbb{R}^{n \times n}$ is infeasible in deep learning. But even simple, especially diagonal, approximations of B are useful: Adam [21] is motivated as a “conservative” (due to the square root) approximation of the empirical FIM’s diagonal. For *feed-forward* neural networks, a more accurate yet computationally feasible approximation of any preconditioner $B \in \mathcal{B}$ can be obtained through Kronecker-factored Approximate Curvature (KFAC) [28]. KFAC provides a tractable preconditioner $\hat{B} \approx B$ through two major approximations:

- (a) \hat{B} is *block-diagonal*, where each block corresponds to weights of a single layer, allowing for a blockwise inversion of \hat{B} .
- (b) Each block \hat{B}_l is the *Kronecker-product* of two smaller matrices, allowing for a factor-wise inversion of \hat{B}_l .

For (b), consider the l th layer of f_θ with weight matrix $W \in \mathbb{R}^{n_l \times n_{l-1}}$. Given an input $a \in \mathbb{R}^{n_{l-1}}$, the layer computes pre-activation $s = Wa$ and outputs $\sigma(s)$, where σ is the activation function. The pseudo-gradient $\mathcal{D}W$ is given by $\mathcal{D}W = ga^\top$, where $g = \mathcal{D}s$ is the pseudo-gradient with respect to s . KFAC approximates the block as

$$\begin{aligned} B_l &= \mathbb{E} \left[\text{vec}(\mathcal{D}W) \text{vec}(\mathcal{D}W)^\top \right] = \mathbb{E} \left[(aa^\top) \otimes (gg^\top) \right] \\ &\approx \mathbb{E} [aa^\top] \otimes \mathbb{E} [gg^\top] = A \otimes G, \end{aligned}$$

which can be viewed as an independence assumption between a and g , with uncentered covariance matrices $A := \mathbb{E}[aa^\top]$ and $G := \mathbb{E}[gg^\top]$. With this approximation, any vector $\text{vec}(V)$ can be efficiently preconditioned by B_l^{-1} via the identity

$$B_l^{-1} \text{vec}(V) = \text{vec}(G^{-1} V A^{-1}). \quad (6)$$

We estimate A and G as exponential moving averages and periodically compute updates to A on an entire batch and updates to G on a single sample (see lines 5 and 11 in alg. 1).

RNN-KFAC [27]. The Kronecker-product approximation follows from $\mathcal{D}W = ga^\top$, which holds when W is used once during the forward pass. In recurrent architectures, any weight matrix W is applied repeatedly to compute a new pre-activation $s_t = Wa_t$ from input a_t at any $t \in \{0, \dots, T-1\}$. The pseudo-gradient

$$\mathcal{D}W = \sum_{t=0}^T g_t a_t^\top,$$

⁵We assume this for KFAC applicability; the invariance only requires invertibility [26].

is then a sum of gradient contributions $w_t := \text{vec}(g_t a_t^\top)$, such that

$$B_I = \mathbb{E} \left[\left(\sum_{t=0}^T w_t \right) \left(\sum_{t=0}^T w_t \right)^\top \right] = \sum_{t=0}^T \sum_{s=0}^T \mathbb{E} [w_t w_s^\top].$$

The analogous KFAC approximation

$$\mathbb{E} [w_t w_s^\top] = \mathbb{E} [(a_t a_s^\top) \otimes (g_t g_s^\top)] \approx A_{t,s} \otimes G_{t,s},$$

with $A_{t,s} := \mathbb{E} [a_t a_s^\top]$ and $G_{t,s} := \mathbb{E} [g_t g_s^\top]$, results in the approximation

$$B_I \approx \sum_{t=0}^T \sum_{s=0}^T A_{t,s} \otimes G_{t,s}, \quad (7)$$

for the preconditioner block. This approximation is a sum of Kronecker-products, which we cannot invert efficiently. To obtain a tractable approximation of B_I , we follow Martens et al. [27] and assume

- (a) intertemporal independence: $A_{t,s} \otimes G_{t,s} = 0$, when $t \neq s$.
- (b) stationarity: $A_{t,t} = A_{s,s}$ and $G_{t,t} = G_{s,s}$ for all t, s .

This yields the single Kronecker product approximation

$$B_I \approx T A_{0,0} \otimes G_{0,0}. \quad (8)$$

Following (b), we approximate $A_{0,0}$ with samples of $A_{t,t}$ from all t (same for $G_{0,0}$). Even with these crude approximations, Martens et al. [27] show that the resulting preconditioner performs well. Below, we drop the indices and refer to $A_{0,0}$ as A and $G_{0,0}$ as G .

EKFAC [11]. Computing a dense preconditioner B is impractical. However, the diagonal of B or QBQ^\top , where Q is an orthogonal matrix, can be estimated efficiently as each entry is the variance of a (rotated) partial pseudo-derivative. Based on this observation, George et al. [11] improve the KFAC approximation by re-estimating the diagonal of \hat{B}_I in its eigenbasis. To start, consider the eigendecomposition of \hat{B}_I

$$A \otimes G = Q\Lambda Q^\top = (Q_A \otimes Q_G)(\Lambda_A \otimes \Lambda_G)(Q_A \otimes Q_G)^\top,$$

where $A = Q_A \Lambda_A Q_A^\top$, and $G = Q_G \Lambda_G Q_G^\top$. We see that the Kronecker-product structure transfers to Q and Λ . Because the diagonal of B_I can be estimated cheaply, we can remove the Kronecker-product assumption on Λ and fit a general diagonal matrix \tilde{D}

$$\min_{\tilde{D} = \text{diag}(\tilde{d}_1, \dots, \tilde{d}_{n_I \times n_{I-1}})} \|B_I - Q\tilde{D}Q^\top\|_F^2, \quad (9)$$

to best approximate B_I in the Frobenius norm. The minimization is solved by $\tilde{d}_i^* = q_i^\top B_I q_i$, where q_i denotes the i th column vector of Q [11, 24].⁶ This ‘‘solution’’ is inaccessible as B_I is unknown but \tilde{d}_i^* can be replaced by a Monte Carlo approximation d_i during the backward pass of pseudo-gradients (see eq. 10). The EKFAC approximation can be summarized as

$$\begin{aligned} \hat{B}_I &= Q \text{diag}(d_1, \dots, d_{n_I \times n_{I-1}}) Q^\top, \\ \text{where } Q &= Q_A \otimes Q_G, \\ d_i &\approx \tilde{d}_i^* = \mathbb{E} \left[(q_i^\top \text{vec}(\mathcal{D}W))^2 \right]. \end{aligned} \quad (10)$$

EKFAC was first introduced in the context of correcting the KFAC approximation of the FIM of a probability distribution, parameterized with a feed-forward or convolutional neural network. We

⁶ \tilde{d}_i^* not only minimizes the Frobenius loss, but several sensible loss functions [24].

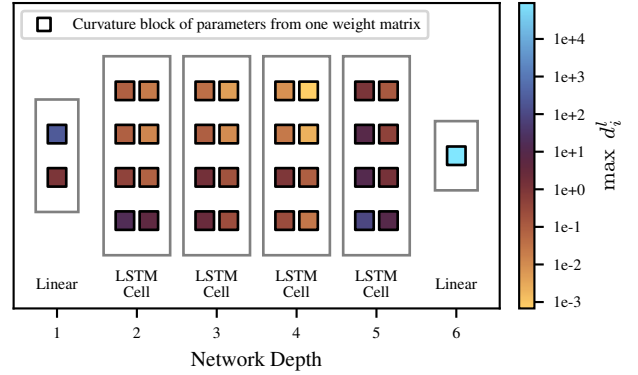


Figure 2: Magnitude of largest eigenvalues differs across blocks (end of training).

highlight that EKFAC is applicable to (i) any $B \in \mathcal{B}$ and (ii) neural network architectures with weight-sharing. Consequently, EKFAC also corrects for the additional RNN-KFAC assumptions (eq. 8).

Damping scheme. We can invert the EKFAC approximation via its eigendecomposition: $\hat{B}_I^{-1} = QD^{-1}Q^\top$. Inverting \hat{B} directly is usually unstable, as even the true preconditioner often has many eigenvalues close to zero. It is common practice, to instead invert $\hat{B} + \lambda \mathbb{I}$, where the damping hyperparameter $\lambda > 0$ often has a significant effect on optimization performance [3, 28, 30]. We find that on our problem and architecture, choosing the same coefficient λ for each block \hat{B}_I leads to over- or under-regularization of different blocks, as the scale of the blocks’ eigenspectra varies significantly among them (fig. 2). Further, we do not find the adaptive damping scheme of George et al. [11, App. C] to alleviate the issue sufficiently. The scheme uses true eigenvalues Λ_A, Λ_G to adjust the effective damping strength. We propose a new damping scheme, that is based on the optimal scale D instead.

As any $B \in \mathcal{B}$ is a covariance matrix, we view damping as *shrinking* a covariance estimator [23]. For a block-diagonal estimator \hat{B} , we suggest shrinking any block $\hat{B}_I \in \mathbb{R}^{N \times N}$ linearly to

$$\hat{B}_I \leftarrow (1 - \rho) \hat{B}_I + \rho \frac{\text{tr}(B_I)}{N} \mathbb{I}_N. \quad (11)$$

The shrinkage target $\text{tr}(B_I)/N$ is block-dependent, while the shrinkage intensity $\rho \in (0, 1)$ is a shared hyperparameter. Because

$$\text{tr}(B_I) = \text{tr}(Q^\top B_I Q) = \text{tr}(D^*) \approx \text{tr}(D),$$

we can estimate the trace without imposing the Kronecker-product assumption.

3.3 Preconditioning the deep hedging problem

We now construct a second-order optimization scheme for deep hedging by preconditioning with a Kronecker-factored matrix. Unlike the related RL setting [20, 36, 40], preconditioning with the FIM is not applicable here, as actions are not randomized, i.e., θ does not parameterize a probability distribution.⁸ However, we can

⁷Here, D_I is a dense matrix of shape $n_I \times n_{I-1}$, as storing this is more efficient than a diagonal matrix of shape $(n_I n_{I-1}) \times (n_I n_{I-1})$ as in Equation (10).

⁸In deep hedging, the optimal policy is deterministic, and the availability of analytical loss function gradients removes the training advantages of probabilistic actions.

Algorithm 1: KFAC for Deep Hedging (DH-KFAC)

Input: samples $(I_t)_{t \geq 0}$; N^{cov} , N^{evd} , β^{TR} , ρ_0^{TR} , β^F , β^D , β^{mom}
Initialize: θ , ∇_l^{avg} , A_l , G_l , D_l , ρ^{TR}

- 1 **for** each iteration i and mini-batch of paths $(I_t)_{t \geq 0}$ **do**
- 2 Compute $u = (u_t)_{t < T}$ with π_θ on each $(I_t)_{t < T}$
- 3 **if** $i \bmod N^{\text{cov}} = 0$ **then** // during forward
 - 4 **for** each layer l **do** // update A_l
 - 5 $A_l \leftarrow \beta^F A_l + (1 - \beta^F) T^{-1/2} \sum_t \mathbb{E}_{\text{batch}} [a_t^l a_t^{l \top}]$
- 6 Sample a *single* path with actions u from mini-batch
- 7 Compute H_u and Cholesky factor L // eq. (12)
- 8 $\ell^{\text{pseudo}} \leftarrow \langle LZ, u \rangle$, where $Z \sim N(0, \mathbb{I})$
- 9 $g \leftarrow \nabla_\theta \ell^{\text{pseudo}}$
- 10 **for** each layer l **do** // update G_l and D_l
 - 11 $G_l \leftarrow \beta^F G_l + (1 - \beta^F) T^{-1/2} \sum_t g_t^l g_t^{l \top}$
 - 12 $D_l \leftarrow \beta^D D_l + (1 - \beta^D) \left(Q_{G_l}^\top \text{mat}(g_l) Q_{A_l} \right)^2$
- 13 **if** $i \bmod N^{\text{evd}} = 0$ **then**
 - 14 Compute eigenvectors Q_{A_l} and Q_{G_l} from A_l and G_l
 - 15 Compute loss \mathcal{L} and gradient $\nabla \leftarrow \nabla \mathcal{L}(\theta)$ // backward
 - 16 **for** each layer l **do** // precondition gradient
 - 17 $\nabla_l^{\text{pre}} \leftarrow Q_{G_l}^\top \text{mat}(\nabla_l) Q_{A_l}$
 - 18 $\nabla_l^{\text{pre}} \leftarrow \nabla_l^{\text{pre}} \oslash ((1 - \varrho) D_l + \varrho \text{mean}(D_l))$
 - 19 $\nabla_l^{\text{pre}} \leftarrow Q_{G_l} \nabla_l^{\text{pre}} Q_{A_l}^\top$
 - 20 $\eta \leftarrow \min \left\{ \sqrt{\rho^{\text{TR}} / \sum_l \langle \text{vec}(\nabla_l^{\text{pre}}), \nabla_l \rangle}, \eta^{\text{max}} \right\}$
 - 21 $\rho^{\text{TR}} \leftarrow \beta^{\text{TR}} \rho^{\text{TR}}$ // decrease trust-region [3]
 - 22 $\nabla_l^{\text{avg}} \leftarrow \beta^{\text{mom}} \nabla_l^{\text{avg}} + \nabla_l^{\text{pre}}$ // momentum
 - 23 $\theta \leftarrow \theta - \eta \nabla^{\text{avg}}$ // update parameters

construct a GGN preconditioner by decomposing the computation of $\mathcal{L}(\theta)$ into a model- and a loss function. A valid GGN decomposition can be defined by treating the tuple $\{\Gamma_T, C_T\}$ as the model output because the per-sample loss function is then convex in this model output. In practice, we find that this decomposition leads to subpar results as the inner Hessian is of rank 1. To obtain a richer curvature model, we define the $d \times T$ -dimensional vector of concatenated hedges $u = \{u_0, \dots, u_{T-1}\}$ as the model output. When viewing eq. (3) as a function of u directly, the per-sample loss function is convex in u . Note that this neglects that through the action recurrence, components in the output vector u depend non-linearly on each other. This additional approximation is in the same spirit as standard GGN approximations [29, 35] as we ignore all second-order interactions that arise within the network.

For the gradient, we use an L1 transaction costs model (eq. 3) to reflect real-world market frictions. For the inner Hessian, a differentiable L2-type transaction costs model is more suitable (better conditioning). We therefore compute the inner Hessian not from eq. (3), but from the pathwise surrogate loss

$$\ell(u) = \gamma (\Gamma_T(u) - \psi(x) - M)^2 + \sum_{t=0}^{T-1} \sum_{i=1}^d \tilde{c}^{(i)} (u_t^{(i)})^2,$$

where M is the mini-batch average of the hedged PnL $(\Gamma_T(u) - \psi(x))$, whose dependence on the single path with action u we neglect. The

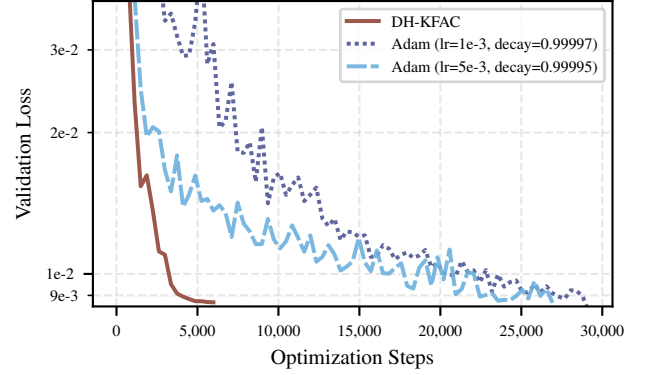


Figure 3: Validation loss during training.

vector $\tilde{c} \in \mathbb{R}^d$ denotes the instrument-wise L2 transaction costs, which we set to $\tilde{c} = 8c$ in our experiments. We denote by H_u the Hessian of $\ell(u)$ and by B^{DH} the proposed GGN-type preconditioner given by

$$B^{\text{DH}} = \mathbb{E} \left[J_{u,\theta}^\top H_u J_{u,\theta} \right]$$

$$H_u = 2\gamma r_{.,T} (r_{.,T})^\top + 2 \text{diag}([\tilde{c}, \dots, \tilde{c}]), \quad (12)$$

where $J_{a,\theta}$ is the (pathwise) Jacobian of the output vector u with respect to θ , and $r_{.,T} = \{r_{0,T}, \dots, r_{T-1,T}\}$ denotes the concatenated returns corresponding to the concatenated actions u .

Our proposed preconditioner is not the only reasonable choice from \mathcal{B} , but it outperforms alternatives we tested in preliminary experiments. Alg. 1 summarizes our second-order optimization scheme for deep hedging (DH-KFAC). Most individual steps are well known from KFAC [3, 28], EKfAC [11], RNN-KFAC [27], or pseudo-gradient sampling [12], but their composition is new. Other novel contributions include the deep hedging preconditioner used in line 7 and the damping scheme in line 18. The step size selection with decaying trust-region size (lines 20-21) is from Ba et al. [3].

4 EXPERIMENTS

4.1 Setup

In this section, we compare our second-order scheme with Adam [21] on training a deep hedging model. We consider hedging a cliquet option in the Heston model [16] and analyze the resulting hedging strategies. With stochastic volatility we can test how well the model learns to use options to hedge volatility risk. In our discrete time setting with transaction costs, perfect hedging is not possible. In the Heston model the price process and volatility satisfy

$$dx_s = x_t \sqrt{v_t} dB_s$$

$$dv_s = \kappa(\theta - v_s) ds + \xi \sqrt{v_s} dW_s,$$

where we assume no drift and choose parameters $x_0 = 1$, $\kappa = 8$, $v_0 = \theta = 0.0625$, $\xi = 1.0$, and correlation $\rho = -0.7$ for Brownian motions B and W . For training, we simulate 700,000 paths [4] for $T = 240$ steps, where each step corresponds to a time increment of $\Delta s = 1/250$. At each step, we price the 19 vanilla options on the

floating grid (fig. 1) using the StochVolModels library [38].⁹ The cliquet has maturity T , cap $\mu = 0.015$, and reset dates $\tau_1 = 20$, $\tau_2 = 40, \dots, \tau_{12} = T$. We assume transaction costs of $c^{(1)} = 1e-4$, and $c^{(i)} = 1e-2$ for $i > 1$, reflecting that delta hedging is cheaper than hedging in options. We set the risk aversion to $\gamma = 1000$.¹⁰

As outlined in section 2.2, we train a recurrent neural network with additional action recurrence (eq. 5). Input features I_t consist of an encoding of time t , spot values x_t and $x_{\max\{\tau_i \leq t\}}$, true volatility v_t , and the cliquet’s payoff if it matured at time t . We process inputs I_t and u_t linearly via $W^I I_t + W^u u_{t-1} + b$ with weight matrices W^I, W^u and bias b . This layer is followed by four residually stacked blocks, where each block applies an RMSNorm [41] and an LSTM cell of dimension 32. Finally, we pass outputs to a linear layer with output dimension d , a symexp activation [13],¹¹ and a masking layer that sets components of output u_t to zero whenever that hedge is not available. We carefully initialize the last layer with zero bias and down-scaled (factor of $1e-3$) [2], He-initialized [15] weights.

We compare our second-order scheme to Adam. For both methods, we grid search hyperparameters and report the best choices below. We find that good architectural and initialization choices (see above) generally benefit both algorithms, though DH-KFAC is more robust to normalizations [see also 3]. We increase Adam’s learning rate linearly during the first epoch and decay it exponentially afterwards (see values in fig. 3). Similarly, DH-KFAC’s trust-region size is decayed with $\beta^{\text{TR}} = 0.997$ each step and initialized at $\rho_0^{\text{TR}} = 1e-3$. We train both methods with a batch size of 2048. We find that Adam requires relatively large batch sizes, which we attribute to the ill-conditioning of the pathwise loss (section 2.3). KFAC is known to work well with large batch sizes [3] and is therefore well-suited to deep hedging. For Adam, we clip gradients such that $\|\nabla \mathcal{L}(\theta)\|_2 \leq 1$. For DH-KFAC, we set $\rho = 5e-4$, $\beta^{\text{mom}} = 0.92$, and $\beta^D = \beta^F = 0.95$.

4.2 Results

Optimization performance. Fig. 3 visualizes the per-iteration optimization progress. We stop training once a given validation loss target is reached. DH-KFAC progresses significantly faster than Adam and only requires about 25% of Adam’s number of steps to reach the targeted loss level. We find that for our small network the per-iteration speedup decreases total training wall-clock time, despite our DH-KFAC implementation not being optimized. For larger networks, distributed computing and performance optimizations are important [3, 39]. In deep hedging, the costs of forward- and backward pass are large relative to the number of parameters, so we expect the KFAC overhead to be smaller than in non-recurrent architectures.¹² In our experiments, we amortize the KFAC computations at rates $N^{\text{cov}} = 5$, $N^{\text{evd}} = 25$.

⁹In the format $\{\tau_i : K^i/x_t\}$ with multiple strikes per maturity, the grid is: {10 : [0.99, 1.0, 1.01]}, {20 : [0.97, 0.99, 1.0, 1.01, 1.03]}, {40 : [0.95, 1.0, 1.05]}, {80 : [0.91, 1.0, 1.09]}, {120 : [0.85, 0.95, 1.0, 1.05, 1.15]}.

¹⁰The choice of the risk aversion coefficient γ determines what hedging strategies are optimal and it has to be tuned to underlying preferences in practice. We chose γ such that the learned hedge clearly shows the impact of option hedging: hedging policies trained with a smaller γ rely more on cheap delta hedging. With our choices for γ and c , transaction costs make up roughly 20% of the loss at the end of training.

¹¹ $\text{symexp}(x) := \text{sign}(x) (\exp |x| - 1)$ for $x \in \mathbb{R}$.

¹²For perspective, Ueno et al. [39] reduce KFAC’s update cost to a multiple of 1.89 of SGD’s cost in distributed ResNet50 training.

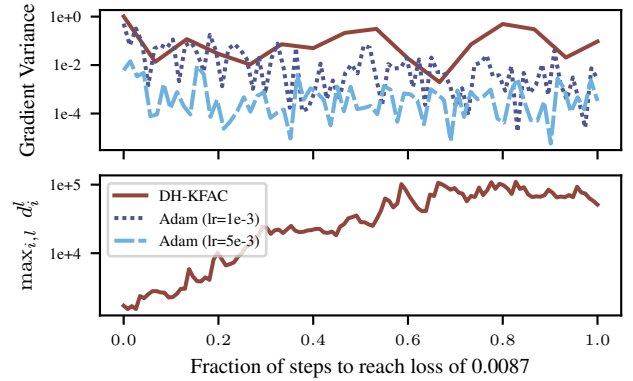


Figure 4: Gradient variance and largest eigenvalue.

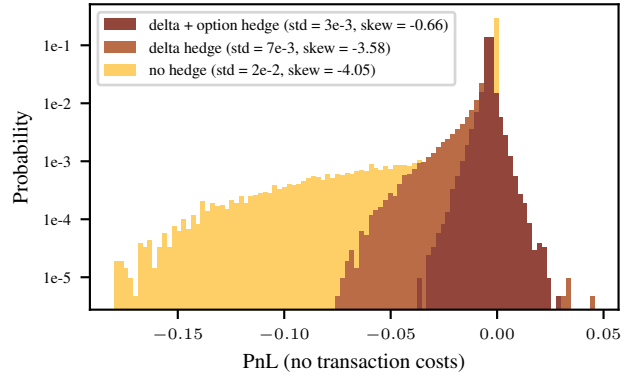


Figure 5: PnL histogram (log scale).

The speedup in per-iteration progress suggests that our second-order scheme can better deal with the loss function’s curvature. The top plot in fig. 4 shows the variance of a batch of *unconditioned* single-sample gradients, i.e., the trace of their empirical covariance matrix. We see that Adam’s optimization path goes through regions of the loss surface with lower gradient variance than DH-KFAC’s. The bottom plot in fig. 4 shows that the largest eigenvalue of our preconditioner increases for most of of training. These observations seem to indicate that DH-KFAC allows for entering high-curvature regions of the loss surface. We leave a precise analysis in terms of *preconditioned sharpness* [8] for future work.

Learned hedging policy. We analyze the learned hedging strategy on an independent test set of 70,000 paths. Here, the model was DH-KFAC-trained, but we eventually reach the same conclusions for Adam-trained models. Fig. 5 visualizes the distribution of the terminal PnL ($\Gamma_T - \psi(x)$) and compares it to the unhedged PnL and the PnL obtained when removing all option hedges. The learned hedging policy significantly reduces PnL variance, primarily with delta hedging. Including option hedging reduces the PnL’s standard deviation by another 50% and increases the skewness of the PnL distribution significantly: the model hedges in vanilla options to protect against tail scenarios. Fig. 6 reinforces this conclusion. It visualizes the distribution of the delta- and an option hedge over time. The visualized option hedge is in a 20-step call option with

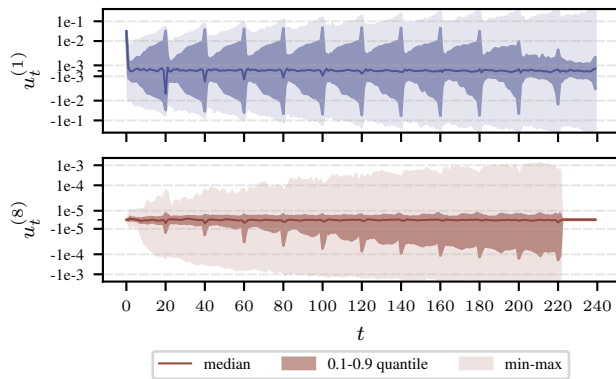


Figure 6: Delta hedge (top) and single option hedge (bottom).

relative strike of 1.01, which lines up closely with the cliquet’s 20-step return cap at 0.015. We see that hedging activity in both instruments increases around the reset dates. For the call, this is when its maturity aligns with the next cliquet fixing date.

5 CONCLUSION

We proposed a second-order scheme for optimizing deep hedging models. We demonstrated that preconditioning gradients with a block-diagonal, Kronecker-factored approximation of the generalized Gauss Newton matrix significantly speeds up per-iteration optimization progress. Beyond the practical use of our algorithm, our paper provides a new perspective on standard deep hedging optimization. This lens of curvature may for instance be useful in the design of whitening layers [9] as we find our algorithm to still perform well when setting $G = \mathbb{I}$. Beyond deep hedging, our approach of leveraging second-order information through a differentiable environment is, with modification of the preconditioner, applicable to other differentiable control and RL problems.

REFERENCES

- [1] Shun-ichi Amari. 1998. Natural Gradient Works Efficiently in Learning. *Neural Computation* 10, 2 (1998), 251–276.
- [2] Marcin Andrychowicz, Anton Raichuk, Piotr Stańczyk, Manu Orsini, Sertan Girgin, Raphael Marinier, Léonard Hussenot, Matthieu Geist, Olivier Pietquin, Marcin Michalski, Sylvain Gelly, and Olivier Bachem. 2020. *What Matters In On-Policy Reinforcement Learning? A Large-Scale Empirical Study*. arXiv:2006.05990
- [3] Jimmy Ba, Roger Grosse, and James Martens. 2017. Distributed Second-Order Optimization Using Kronecker-Factored Approximations. In *International Conference on Learning Representations*.
- [4] Mark Broadie and Özgür Kaya. 2006. Exact Simulation of Stochastic Volatility and Other Affine Jump Diffusion Processes. *Operations Research* 54, 2 (2006), 217–231.
- [5] Hans Buehler. 2017. *Statistical Hedging*. SSRN: 2913250.
- [6] Hans Buehler, Lukas Gonon, Josef Teichmann, and Ben Wood. 2019. Deep Hedging. *Quantitative Finance* 19, 8 (2019), 1271–1291.
- [7] Alexandre Carbonneau. 2021. Deep Hedging of Long-Term Financial Derivatives. *Insurance: Mathematics and Economics* 99 (2021), 327–340.
- [8] Jeremy Cohen, Behrooz Ghorbani, Shankar Krishnan, Naman Agarwal, Sourabh Medapati, Michal Badura, Daniel Suo, David Cardoze, Zachary Nado, George Dahl, and Justin Gilmer. 2024. *Adaptive Gradient Methods at the Edge of Stability*. arXiv:2207.14484
- [9] Guillaume Desjardins, Karen Simonyan, Razvan Pascanu, and Koray Kavukcuoglu. 2015. Natural Neural Networks. In *Advances in Neural Information Processing Systems*, Vol. 28. Curran Associates, Inc., 2071–2079.
- [10] Jeffrey Elman. 1990. Finding Structure in Time. *Cognitive Science* 14, 2 (1990), 179–211.
- [11] Thomas George, César Laurent, Xavier Bouthillier, Nicolas Ballas, and Pascal Vincent. 2018. Fast Approximate Natural Gradient Descent in a Kronecker Factored Eigenbasis. In *Advances in Neural Information Processing Systems*, Vol. 31. Curran Associates, Inc., 9573–9583.
- [12] Roger Grosse. 2022. Lecture Notes on Neural Net Training Dynamics (Chapter 3: Metrics). https://www.cs.toronto.edu/~rgrosse/courses/csc2541_2022/readings/L03_metrics.pdf
- [13] Danijar Hafner, Jurgis Pasukonis, Jimmy Ba, and Timothy Lillicrap. 2023. *Mastering Diverse Domains through World Models*. arXiv:2301.04104
- [14] Ben Hambly, Renyuan Xu, and Huining Yang. 2023. Recent Advances in Reinforcement Learning in Finance. *Mathematical Finance* 33, 3 (2023), 437–503.
- [15] Kaiming He, Xiangyu Zhang, Shaoqing Ren, and Jian Sun. 2015. Delving Deep into Rectifiers: Surpassing Human-Level Performance on ImageNet Classification. In *International Conference on Computer Vision*. IEEE, 1026–1034.
- [16] Steven Heston. 1993. A Closed-Form Solution for Options with Stochastic Volatility with Applications to Bond and Currency Options. *The review of financial studies* 6, 2 (1993), 327–343.
- [17] Sepp Hochreiter and Jürgen Schmidhuber. 1997. Long Short-Term Memory. *Neural Computation* 9, 8 (1997), 1735–1780.
- [18] Blanka Horvath, Josef Teichmann, and Zan Žurič. 2021. Deep Hedging under Rough Volatility. *Risks* 9, 7 (2021), 138.
- [19] Herbert Jaeger. 2002. *Tutorial on training recurrent neural networks, covering BPPT, RTRL, EKF and the "echo state network" approach*. Vol. 5. GMD-Forschungszentrum Informationstechnik Bonn.
- [20] Sham M Kakade. 2001. A Natural Policy Gradient. In *Advances in Neural Information Processing Systems*, Vol. 14. MIT Press, 1531–1538.
- [21] Diederik Kingma and Jimmy Ba. 2015. Adam: A Method for Stochastic Optimization. In *International Conference on Learning Representations*.
- [22] Agustinus Kristiadi, Felix Dangel, and Philipp Hennig. 2023. The Geometry of Neural Nets’ Parameter Spaces Under Reparametrization. In *Advances in Neural Information Processing Systems*, Vol. 36. Curran Associates, Inc., 17669–17688.
- [23] Olivier Ledoit and Michael Wolf. 2004. A Well-Conditioned Estimator for Large-Dimensional Covariance Matrices. *Journal of Multivariate Analysis* 88, 2 (2004), 365–411.
- [24] Olivier Ledoit and Michael Wolf. 2021. Shrinkage Estimation of Large Covariance Matrices: Keep It Simple, Statistician? *Journal of Multivariate Analysis* 186 (2021), 104796.
- [25] Eva Lütkebohmert, Thorsten Schmidt, and Julian Sester. 2022. Robust Deep Hedging. *Quantitative Finance* 22, 8 (2022), 1465–1480.
- [26] James Martens. 2020. New Insights and Perspectives on the Natural Gradient Method. *Journal of Machine Learning Research* 21, 146 (2020), 1–76.
- [27] James Martens, Jimmy Ba, and Matt Johnson. 2018. Kronecker-Factored Curvature Approximations for Recurrent Neural Networks. In *International Conference on Learning Representations*.
- [28] James Martens and Roger Grosse. 2015. Optimizing Neural Networks with Kronecker-factored Approximate Curvature. In *International Conference on Machine Learning (Proceedings of Machine Learning Research, Vol. 37)*. PMLR, 2408–2417.
- [29] James Martens and Ilya Sutskever. 2011. Learning Recurrent Neural Networks with Hessian-Free Optimization. In *International Conference on Machine Learning*, 1033–1040.
- [30] James Martens and Ilya Sutskever. 2012. Training Deep and Recurrent Networks with Hessian-Free Optimization. In *Neural Networks: Tricks of the Trade*. Vol. 7700. Springer, 479–535.
- [31] Shakir Mohamed, Mihaela Rosca, Michael Figurnov, and Andriy Mnih. 2020. Monte Carlo Gradient Estimation in Machine Learning. *Journal of Machine Learning Research* 21, 132 (2020), 1–62.
- [32] Phillip Murray, Ben Wood, Hans Buehler, Magnus Wiese, and Mikko Pakkanen. 2022. Deep Hedging: Continuous Reinforcement Learning for Hedging of General Portfolios across Multiple Risk Aversions. In *ACM International Conference on AI in Finance*. ACM, 361–368.
- [33] Antonio Orvieto, Samuel Smith, Albert Gu, Anushan Fernando, Çağlar Gülçehre, Razvan Pascanu, and Soham De. 2023. Resurrecting Recurrent Neural Networks for Long Sequences. In *International Conference on Machine Learning (Proceedings of Machine Learning Research, Vol. 202)*. PMLR, 26670–26698.
- [34] Johannes Ruf and Weiguan Wang. 2020. Neural Networks for Option Pricing and Hedging: A Literature Review. *Journal of Computational Finance* (2020).
- [35] Nicol Schraudolph. 2002. Fast Curvature Matrix-Vector Products for Second-Order Gradient Descent. *Neural Computation* 14, 7 (2002), 1723–1738.
- [36] John Schulman, Sergey Levine, Pieter Abbeel, Michael Jordan, and Philipp Moritz. 2015. Trust Region Policy Optimization. In *International Conference on Machine Learning (Proceedings of Machine Learning Research, Vol. 37)*. PMLR, 1889–1897.
- [37] Martin Schweizer. 1995. Variance-Optimal Hedging in Discrete Time. *Mathematics of Operations Research* 20, 1 (1995), 1–32.
- [38] Artur Sepp and Parviz Rakhmonov. 2024. *Log-Normal Stochastic Volatility Model with Quadratic Drift*. SSRN: 2522425.
- [39] Yuichiro Ueno, Kazuki Osawa, Yohei Tsuji, Akira Naruse, and Rio Yokota. 2020. Rich Information Is Affordable: A Systematic Performance Analysis of Second-order Optimization Using K-FAC. In *ACM SIGKDD International Conference on*

Knowledge Discovery & Data Mining. ACM, 2145–2153.

- [40] Yuhuai Wu, Elman Mansimov, Roger Grosse, Shun Liao, and Jimmy Ba. 2017. Scalable Trust-Region Method for Deep Reinforcement Learning Using Kronecker-factored Approximation. In *Advances in Neural Information Processing Systems*, Vol. 30. Curran Associates, Inc., 5285–5294.
- [41] Biao Zhang and Rico Sennrich. 2019. Root Mean Square Layer Normalization. In *Advances in Neural Information Processing Systems*, Vol. 32. Curran Associates, Inc., 12360–12371.

DISCLAIMER

This paper was prepared for information purposes by the Quantitative Research group of JPMorgan Chase & Co and its affiliates (“JP Morgan”), and is not a product of the Research Department of JP Morgan. JP Morgan makes no representation and warranty whatsoever and disclaims all liability, for the completeness, accuracy or reliability of the information contained herein. This document is not intended as investment research or investment advice, or a recommendation, offer or solicitation for the purchase or sale of any security, financial instrument, financial product or service, or to be used in any way for evaluating the merits of participating in any transaction, and shall not constitute a solicitation under any jurisdiction or to any person, if such solicitation under such jurisdiction or to such person would be unlawful.